Detection of Prostate Cancer from Multiparametric Magnetic Resonance Imaging

Anonymous Author(s)
Affiliation
Address
email

Abstract

In this study, a multiparametric magnetic resonance image (MRI) based technique of detecting prostate cancer is developed. A machine learning algorithm, based on random forest is used to classify the normal and cancer regions. Three features extracted from dynamic contrast enhanced MRI and two features extracted from diffusion tensor MRI is used to train the classifier. The classifier is trained to detect prostate cancer in the peripheral zone and using the trained classifier, cancer probability map is generated for the entire prostate gland.

1 Introduction

As the second leading cause of cancer-related death among males [1] prostate cancer patients require non-invasive detection and staging. Mortality is often due to the metastasis of cancer from prostate to bones which happens only in a small number of patients. In fact, prostate cancer, if detected prior to spreading to bones, can be controlled. Since the existing diagnosis techniques can not adequately determine the stage of prostate cancer, radical prostatectomy is generally used in treating prostate cancer [2], even for patients with pathologically insignificant cancer [3]. This surgery eventually could lead the patient to incontinence and impotence, and other sexual and urinary complications. To assess prostate cancer, biopsy under transrectal ultrasound (TRUS) is used for most of the cases. However, TRUS cannot accurately image prostate cancer, and therefore biopsy protocols suffer from false negatives or under-sampling of major tumors [4]. Therefore, there is growing need for new diagnosis techniques that can identify the location and stage of prostate cancer adequately and non-invasively.

Magnetic resonance imaging (MRI) has proven its ability to visualize the prostate anatomy [5]. However its poor specificity [6] and insufficient sensitivity [7] made T2-weighted MRI less applicable for diagnosis and grading of prostate tumors. Since mid-1980s, different MRI modalities have been investigated for the assessment of prostate cancer [6]. Particularly, diffusion MRI (DTI) has shown very promising results and correlation with Gleason grade [8]. A number of recent MRI studies have demonstrated that the detection and grading of prostate cancer can be improved through the addition of DTI [9] and dynamic contrast enhanced imaging (DCE) [10] to an MRI staging exam. Diffusion imaging characterize the de-phasing of the MR signal by molecular diffusion. Prostate cancer changes the regular pattern of distribution of prostate gland and this irregular distribution and increased cellular density results in lower diffusivity (D) and decreased aparent diffusion coefficient (ADC) value in DTI. The structural changes also alters the uptake of contrast agent in dynamic contrast enhanced imaging (DCE). In DCE MRI, an contrast agent of small molecular weight is injected into the patient, and the increase in signal intensity is measured from fast T1-weighted images. The rate of enhancement depends on the vascular volume and permeability of the vessels, and the magnitude depends on extravascular/extracellular leakage space. Studies have shown that the rate of contrast enhancement is higher and faster in the cancer affected areas [11]. However, each modality has their own advantages and disadvantages, and therefore no one modality has proven

to be the the perfect diagnosis method for prostate cancer detection. The best characterization of prostate cancer will most likely result from a multiparametric MRI exam using 3T magnetic resonance scanners [6]. The most recent reported results show that multiparametric MRI at 3T, which combines dynamic contrast enhanced (DCE) imaging with diffusion weighted imaging provides the highest performance in terms of area under receiver operating characteristic (ROC) curve [2].

In this study, a machine learning approach based on random forest is used to develop a multiparametric magnetic resonance imaging based technique for detection of prostate cancer. Features extracted from dynamic contrast enhanced MRI and diffusion tensor MRI is used to train and test the classifier. Based on the classification, cancer probability map is generated for the entire prostate gland using the standard Jet colormap, where hot color represents high probability of cancer.

2 Materials and methods

2.1 Prostate MRI data

For this study, I used MRI data from two different studies and both of them was approved by Clinical Research Ethics Board of our institution. One dataset was from a biopsy study and another dataset was from patients scheduled for radial prostatectomy.

2.1.1 Biopsy data

The biopsy dataset was collected in 2009 from 29 patients with a high clinical suspicion for prostate adenocarcinoma due to an elevated prostate specific antigen (PSA) and/or palpable prostatic nodule. Average PSA was 8.5 ng/mL (range: 0.9415 ng/mL). Before entering the study, each patient gave their written consent to take part in the study. The biopsies were performed under local anesthetic and the number of biopsies obtained from the peripheral zone (PZ) was determined by prostate gland size. In patients with a prostate gland of 30 cc or less, eight biopsies (base: right and left; midgland: right lateral, left lateral, right medial, left medial; apex: right and left) were taken. For prostate glands ranging from 31 to 60 cc, 10 biopsies (base: right lateral, left lateral, right medial, left medial; midgland; and apex biopsies as above) were obtained. For prostate glands greater than 60 cc, 12 biopsies were obtained (apex: right lateral, left lateral, right medial, left medial; base; and midgland biopsies the same as the 10 biopsy scheme). The dataset included a total of 240 negative biopsy cores and 29 positive biopsy cores. The positive cores were from 10 patients. The histology was interpreted with assignment of the Gleason score by several different experienced anatomic pathologists who practice general and subspecialty uropathology.

2.1.2 Prostatectomy data

The Prostatectomy data used here was obtained in 2010 from a different population than the biopsy cases described above. The patients recruited for this study have not received any therapy before radical prostatectomy. To acquire the whole-mount pathology analysis, the radical prostatectomy specimens were dissected and histopathologically examined in a uniform manner. The specimens were dissected following a minimum of 24-h fixation in 10% buffered formalin. The apical and bladder neck tissue was removed, using 5-mm-thick layers. To cut the prostate gland, a device described in [12] was used and the prostate gland was cut in serial transverse cuts perpendicular to the posterior capsule, at 4-mm intervals, from inferior to superior. This procedure allowed us to obtain reasonably good correspondence between the pathology slices and the MR image slices.

2.1.3 MRI data collection protocol

MRI examinations were performed on a 3 Tesla (T) MRI scanner (Achieva, Philips Healthcare, Best, The Netherlands) and MRI signals were acquired with a combination of an endorectal coil (Medrad, Pittsburgh, PA) and a cardiac phased-array coil (Philips Healthcare, Best, The Netherlands). Fast spin-echo T2-weighted images were acquired using repetition time (TR) of 1851 ms and effective echo time (TE) of 80 ms with 14 cm field of view (FOV) (284×225 matrix). Each slice was 4 mm thick and there was no gap between the slices. From this sequence, 12 axial slices covering the entire gland were then selected to use for the DTI and DCE MRI scans. DTI data were acquired using a diffusion weighted single shot echo planar imaging (EPI) sequence (TR = 2100 ms TE = 74 ms,

FOV = 24 cm, 128×115 matrix, b-value = 0 and 600 s/mm^2 , 18 averages, 6 noncollinear gradient directions). DCE T1-weighted images were acquired using a three-dimensional T1-weighted spoiled gradient echo-sequence (TR/TE = 3.4/1.06 ms, flip angle = 15°, FOV = 24 cm, 256×163 matrix). The contrast agent used here was Gd-DTPA (Magnevist, Berlex Canada). 0.1 mmol/kg of Gd-DTPA was injected with a motorized power injector within 10 s at the rate of 2 mL/s, followed by a 20 mL flush of saline. This resulted in a time resolution of 10.6 s per 12 slices. This resulted in a time resolution of 10.6 s per 12 slices.

The total time of the MRI examination was approximately 45 min. The DTI data were processed off-line to calculate FA and average diffusivity (D) values. Diffusion weighted images were registered to the nonweighted b = 0 image with a mutual information algorithm before calculating the eigenvalues of the diffusion tensor and generating maps of the average diffusivity (D) and fractional anisotropy (FA) with the proprietary DTI processing toolbox PRIDE (Philips Healthcare, Best,The Netherlands). DCE MRI data were processed off-line with software procedures developed in house using Matlab (Math-works, Natick, MA) and Igor Pro (WaveMetrics, Port-land, OR). Pharmacokinetic parameters: volume transfer constant (K^{trans}), fractional volume of the extra-vascular extracellular space(v_e) and fractional plasma volume (v_p), were calculated by fitting the contrast agent concentration versus time curves to the extended Kety model. Fitting was carried out in every pixel of every slice within a region of interest (ROI) encompassing the prostate gland to generate maps of the pharmacokinetic parameter as described by Tofts et al [13].

2.2 Features of DTI and DCE MRI

To calculate the cancer probability, in this work I have used 2 parameters extracted from Diffusion Tensor MRI (DTI) and 3 parameters extracted from Dynamic Contrast Enhanced (DCE) MR images. Diffusion tensor magnetic resonance imaging (DT-MRI) maps the diffusion of hydrogen atoms within water molecules in biological tissues. Diffusion process in tissues depends on its interaction with obstacles (micromolecules, fibres, membranes) and mapping of diffusion pattern can reveal microscopic details about tissue structure and differentiate between normal and diseased tissues. In the presence of a strong magnetic field, this diffusion pattern results in irreversible dephasing of MR signal making diffusion a dominant source of contrast in MRI [14]. In this study, two parameters extracted from DTI is used as feature- apparent diffusion coefficient (ADC) and fractional anisotropy (FA). ADC is an indicator of the reduction in MR signal due to the amount of diffusion. Since diffusion pattern changes in cancer tissues, it results in a decrease in ADC. Fractional anisotropy is a measure of diffusivity differences in different directions, and it is also affected by the diffusion pattern change due to tumors.

In dynamic contrast-enhanced MRI (DCE-MRI), a small molecular weight contrast agent, generally gadolinium-DTPA, is injected into the patient and the distribution of the contrast agent is repeatedly imaged. DCE-MRI has been shown to significantly improve tissue characterization and the pharmacokinetic modeling parameters have shown promising results in differentiating cancer and normal tissue in prostate gland [14]. In this work, three parameters extracted from DCE-MRI is used as feature vectors- volume transfer constant (K^{trans}), fractional volume of the extra-vascular extracellular space(v$_e$) and fractional plasma volume (v$_p$). Depending on the balance between capillary permeability and blood flow in the tissue of interest, the volume transfer constant, K^{trans}, has several physiologic interpretations. In high-permeability situations where flux across the endothelium is flow limited, the transfer constant is equal to the blood plasma flow per unit volume of tissue. In case of low permeability, transfer constant equals to the permeability surface area product between blood plasma and the extra-vascular extra-cellular space, per unit volume of tissue [13]. Fractional plasma volume (v$_p$) is the volume of blood plasma per unit volume of tissue, and v$_e$ is the volume of extra-vascular extra-cellular space per unit volume of tissue.

2.3 Selecting ROI from MRI

The histology slides were examined and the regions of the prostatic carcinoma were outlined with assignment of the Gleason score by an anatomic pathologist with over 20 years of experience. The cutting device used to cut the gland ensured the matching of two-dimensional MRI slices with pathology slides. To relate the ROIs from the DTI and DCE parameter maps with the corresponding pathology slides, the image of the entire prostate gland in the pathology slide and in the parameter

maps were divided into the same number of grids, where the area of each grid was 3.29×3.29 mm^2. Feature vectors are calculated by picking up grid from the peripheral zone of the gland and averaging over the entire grid. Thus each 3.29×3.29 mm^2 area of the gland gave rise to one feature vector. The label or class of the feature vector was selected from the same grid in pathology image, where a class of 1 is assigned if that grid corresponds to a cancer region in pathology image, and class of 0 is assigned if it corresponds to healthy region.

2.4 Classification by random forest

Two features extracted from DTI (ADC and FA) and three features extracted from DCE-MRI (K^{trans}, v_e, v_p) were used to construct a five dimensional feature vector, $x = [ADC, FA, K^{trans}, v_e, v_p]$. Figure 1 shows the inter-relationships among these features. Each image I(i,j) shows feature-i vs. feature-j, where blue dots denote healthy samples and red dots denote cancer samples. As can be seen, the features are highly correlated and therefore they can not be classified by simple linear methods. Hence I used random forest to classify them.

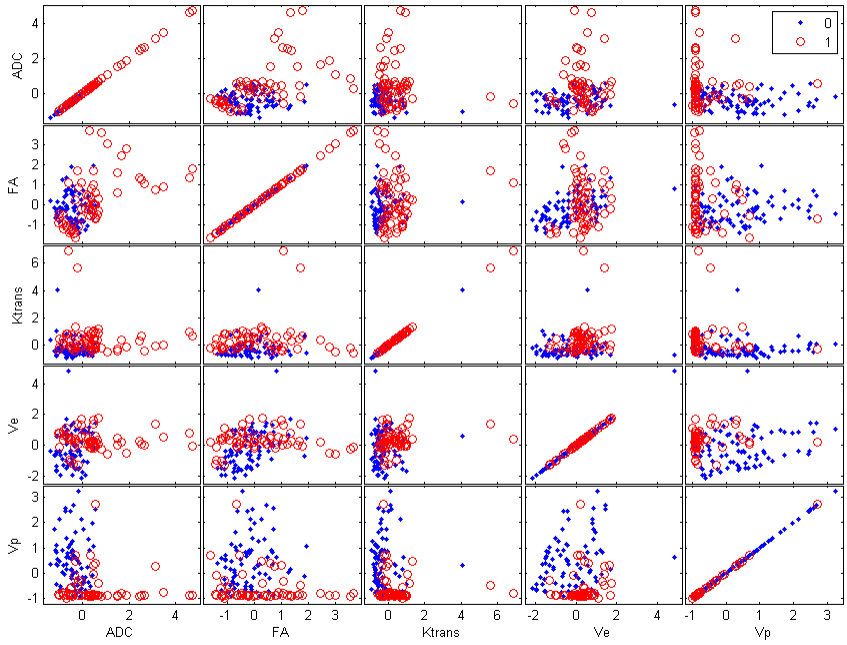

Figure 1: Cancer and normal samples are plotted as a function of features from DTI and DCE. Red dots denote cancer samples and blue dot denotes healthy samples.

Random forest algorithm is applied to classify normal and cancer regions in prostate gland based on these five features. Random forests are an ensemble learning method for classification that operates by constructing a number of bagged decision trees. Each decision tree is constructed from the entire training data or a subset of it. For splitting each node of the tree, all the possibilities of splitting the node is investigated. The split that maximizes the information gain is selected and the node is split into two daughter nodes. Random forest gives its output probability of test data by averaging the probability values given by all of its decision trees. The random forest algorithm in this work follows Breiman's algorithm. In this algorithm, each tree is trained on a bootstrapped sample of the original data set. For growing each tree, each time N-samples were taken with replacement, where N equals the total number of input data. To split each node, two variables at random were considered for splitting. An ensemble of 50 bagged decision trees was trained with a minimum leaf size of three samples.

3 Result Analysis

To study the role of DCE and DTI separately, three classifiers were trained with each method, one classifier with only DTI parameters as feature vectors (ADC and FA), one with only DCE parameters (K^{trans}, v_e, v_p) and one classifier was trained with DTI and DCE parameters together. All features were collected from the peripheral zone of prostate gland and the classifiers were trained to detect the presence of cancer in the peripheral region.

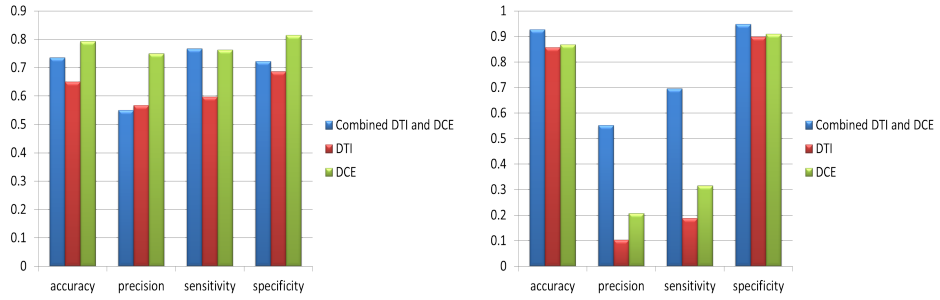

Figure 2: Classification result from Random Forest. The left figure shows the accuracy, precision, sensitivity and specificity for the prostatectomy data. Right figure shows the accuracy, precision, sensitivity and specificity for the biopsy data.

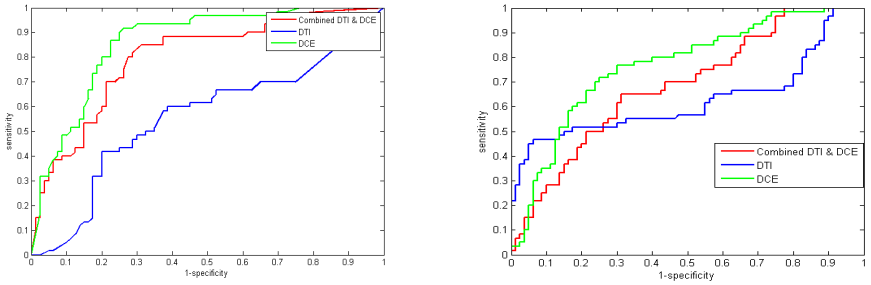

Figure 3: ROC curve for prostatectomy dataset. The left figure is from random forest and right figure is from support vector machine classification.

From the prostatectomy dataset, 140 samples from 4 patients are used to train and test the classifier. All the samples were taken from the peripheral zone of prostate gland and out of 140 samples 60 samples were from cancer regions and remaining 80 were normal samples. The classifiers were trained on a leave-one-patient-out basis. Each time the classifiers were trained on 3 patient data and tested on the remaining patient. The area under receiver operating characteristics (ROC) curve was 0.59 with onlt DTI features, 0.867 with only DCE features and 0.816 with combined DTI and DCE featuers. The combined feature vector resulted in higher area under ROC curve(AUC) than with DTI features alone and was similar to the AUC value found with DCE parameters only.

With the combined feature vector, at the decision threshold of 0.5, 27 tumors were misclassified and 10 normal samples were misclassified as tumors. 103 out of 140 samples were correctly classified with an accuracy of 73.6% and specificity of 72.2%. Optimum threshold was found to be 0.32 with a maximum accuracy of 78.6%. With only DTI parameter, 26 tumors were misclassified and 91 out of 140 samples were correctly classified at decision threshold of 0.5 with accuracy of 65% and specificity of 68.7%. The maximum accuracy (70.7%) was reached at threshold 0.68. With only DCE parameters, 15 tumors were misclassified and 111 out of 140 samples were correctly classified with a specificity of 81.5% and accuracy of 79.3%. Figure 2(left) shows the accuracy, precision, sensitivity and specificity values with DTI, DCE and combined feature vector from prostatectomy dataset.

The biopsy dataset had 272 samples from 29 patients and the classifier was trained and tested one leave-one-patient-out basis. The area under ROC curve (AUC) was found to be 0.844 with DTI features alone, 0.715 with DCE features alone and 0.935 with combined DTI and DCE features. The combined features showed improvement in AUC values than DTI and DCE parameters alone. With combined feature vector, at the decision threshold of 0.5, 252 samples were correctly classified and only 13 cancer samples were misclassified, whereas with DTI and DCE parameters alone, 26 and 23 tumors were misclassified respectively. With combined feature vector, the accuracy was 92.6% with specificity 94.8% and a maximum accuracy of 93.8% was reached at threshold 0.47. With only DTI and DCE parameters the accuracy was 85.7% and 86.8% and specificity was 89.8% and 90.9% respectively. Figure 2(right) shows the accuracy, precision, sensitivity and specificity values from biopsy dataset. For both the dataset, combined feature vector clearly showed improvement in sensitivity over classification with only DTI and DCE feature vectors. With biopsy data, combined feature vector showed improved accuracy and specificity while with prostatectomy data it showed comparable values with classification by DCE feature vector. The increase in sensitivity by combining DTI and DCE features shows the potential of multiparametric MRI in classification. However, the lower specificity and accuracy value in prostatectomy dataset may have arisen due to the fact that the prostatectomy dataset was small. The correct validation of accuracy would be possible with large dataset.

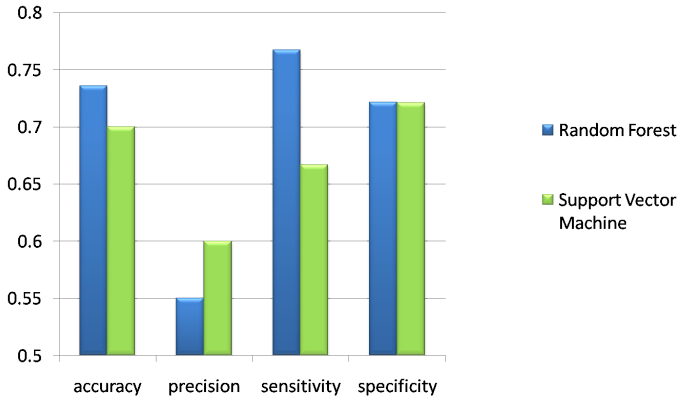

Figure 4: Comparison of classification results from random forest with support vector machine classification.

To compare the results of random forest, the prostatectomy dataset was classified by support vector machine classification (SVM), with a radial basis function as the kernel. The library used here is the publicly available C++ implementation of the SVM algorithms known as LIBSVM (http://www.csie.ntu.edu.tw/ cjlin/libsvm/). Figure 4 shows the accuracy, precision, sensitivity and specificity values resulted from the classification with combined five dimensional feature vector by random forest and SVM. Random forest shows improvement in accuracy, sensitivity and specificity.

The trained random forest classifier was used to generate cancer probability maps for the entire prostate gland. To generate the probability map, feature vectors were constructed from the DCE and DTI parametric maps for each pixel of the gland. These feature vectors were then used as the test samples and each pixel was classified using the trained classifier. The probability scores given to each pixel were plotted using standard Jet colormap to generate cancer probability map of the entire gland. Higher probabilities gave rise to hot colors in the probability map. Figure 5 shows one case where the main pathologic finding was a tumor with Gleason score 3+3 in the left peripheral zone. The corresponding cancer probability map generated by the classifier is shown along with the T2-weighted MR image. The hot spot is outlined in the probability map. The cancer probability map clearly shows higher probability values in the cancer region. However, there are hot spots in central and transitional zones of the gland. This is due to the fact that the classifier was trained only for the peripheral zone, and since the parameter values are different in other zones of the gland, the classifier can not distinguish normal and cancer regions in central or transitional zone of the prostate gland. Figure 6 shows another case where the main pathologic finding was tumor in the left peripheral zone

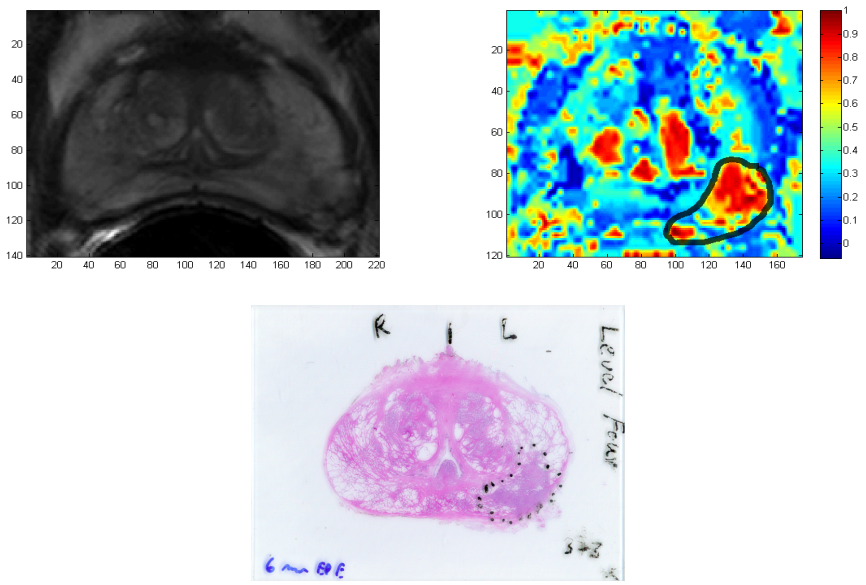

Figure 5: Cancer probability map with corresponding T2-weighted MR image and histopathology slide. The main pathologic finding is tumor in the left peripheral zone with Gleason score 3+3. Corresponding hot spot is outlined in the probability map.

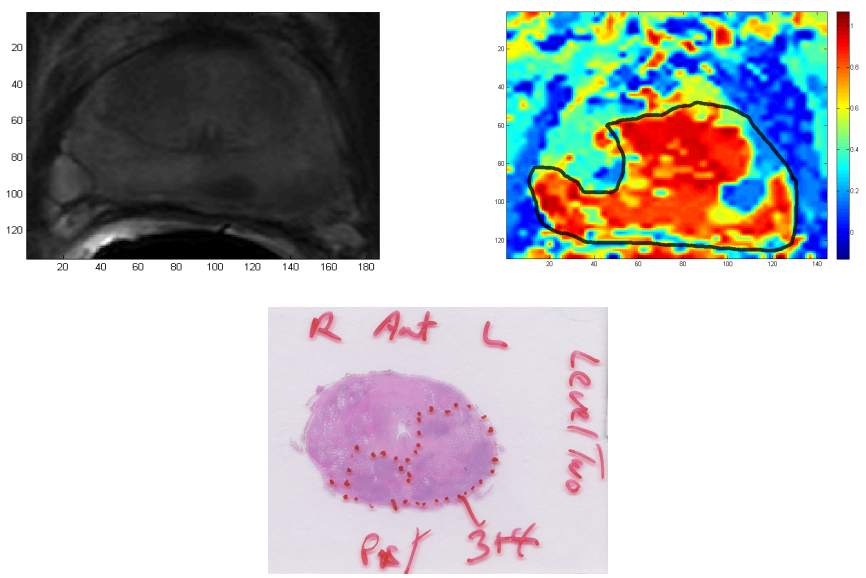

Figure 6: Cancer probability map with corresponding T2-weighted MR image and histopathology slide. The main pathologic finding is tumor in the left peripheral zone with Gleason score 3+4. Corresponding hot spot is outlined in the probability map.

with Gleason score 3+4. The cancer probability map for this slide can also distinguish the tumor region from the surrounding healthy region.

4 Conclusion

A random forest classifier, trained by combination of DCE and DTI MRI features, provided helpful cancer probability maps for detection of prostate cancer. The performance of the method is reported on a biopsy dataset of 29 patients, and on a prostatectomy dataset of 5 patients. The performance of random forest was compared with support vector machine classifier, and random forest proved to be the better choice for prostate cancer detection in terms of accuracy and sensitivity. The generated cancer probability maps for the entire gland can distinguish cancer in the peripheral zone.

References

[1] Jemal, A., Bray, F., Center, M.M., Ferlay, J., Ward, E., Forman, D.: Global cancer statistics. CA:A Cancer Journal for Clinicians **61** (2011) 69–90

[2] Moradi, M., Salcudean, S.E., Chang, S.D., Jones, E.C., Buchan, N., Casey, R.G., Goldenberg, S.L., Kozlowski, P.: Multiparametric MRI maps for detection and grading of dominant prostate tumors. Journal of Magnetic Resonance Imaging **35**(6) (2012) 1403–1413

[3] Steyerberg, E.W., Roobol, M.J., Kattan, M.W., van der Kwast, T.H., de Koning, H.J., Schröder, F.H.: Prediction of indolent prostate cancer:validation and updating of a prognostic nomogram. Journal of Urology **177**(1) (2007) 107–112

[4] Odowd, G.J., Miller, M.C., Orozco, R., Veltri, R.W.: Analysis of repeated biopsy results within 1 year after a noncancer diagnosis. Urology **55**(4) (2000) 553–558

[5] Kurhanewicz, J., Swanson, M.G., Nelson, S.J., Vigneron, D.B.: Combined magnetic resonance imaging and spectroscopic imaging approach to molecular imaging of prostate cancer. Journal of Magnetic Resonance Imaging **16**(4) (2002) 451–463

[6] Kurhanewicza, J., Vignerona, D., Carrollb, P., Coakleya, F.: Multiparametric magnetic resonance imaging in prostate cancer:present and future. Current Opinion in Urology **18**(1) (2008) 71–77

[7] Augustin, H., Fritz, G., Ehammer, T., Auprich, M., Pummer, K.: Accuracy of 3-tesla magnetic resonance imaging for the staging of prostate cancer in comparison to the partin tables. Acta radiologica **50**(5) (2009) 562–569

[8] Hambrock, T., Somford, D.M., Huisman, H.J., van Oort, I.M., Witjes, J.A., Hulsbergen-van de Kaa, A.C., Scheenen, T., Barentsz, J.O.: Relationship between apparent diffusion coefficients at 3.0-t mr imaging and gleason grade in peripheral zone prostate cancer. Radiology **259**(2) (2011) 453–461

[9] Manenti, G., Squillaci, E., Di Roma, M., Carlani, M., Mancino, S., Simonetti, G.: In vivo measurement of the apparent diffusion coefficient in normal and malignant prostatic tissue using thin-slice echo-planar imaging. La radiologia medica **111**(8) (2006) 1124–1133

[10] Villers, A., Puech, P., Mouton, D., Leroy, X., Ballereau, C., Lemaitre, L.: Dynamic contrast enhanced, pelvic phased array magnetic resonance imaging of localized prostate cancer for predicting tumor volume: correlation with radical prostatectomy findings. The Journal of urology **176**(6) (2006) 2432–2437

[11] Noworolski, S., Henry, R., Vigneron, D., Kurhanewicz, J.: Dynamic contrast-enhanced mri in normal and abnormal prostate tissues as defined by biopsy, mri, and 3d mrsi. Magnetic resonance in medicine **53**(2) (2005) 249–255

[12] Drew, B., Jones, E.C., Reinsberg, S., Yung, A.C., Goldenberg, S.L., Kozlowski, P.: Device for sectioning prostatectomy specimens to facilitate comparison between histology and in vivo mri. Journal of Magnetic Resonance Imaging **32**(4) (2010) 992–996

[13] Tofts, P.S., Brix, G., Buckley, D.L., Evelhoch, J.L., Henderson, E., Knopp, M.V., Larsson, H.B., Lee, T.Y., Mayr, N.A., Parker, G.J., et al.: Estimating kinetic parameters from dynamic contrast-enhanced t 1-weighted mri of a diffusable tracer: standardized quantities and symbols. Journal of Magnetic Resonance Imaging **10**(3) (1999) 223–232

[14] Kozlowski, P., Chang, S.D., Jones, E.C., Berean, K.W., Chen, H., Goldenberg, S.L.: Combined diffusion-weighted and dynamic contrast-enhanced mri for prostate cancer diagnosiscorrelation with biopsy and histopathology. Journal of Magnetic Resonance Imaging **24**(1) (2006) 108–113